ЯДЕРНА ФІЗИКА
NUCLEAR PHYSICS

УДК 539.172.4:523.51 https://doi.org/10.15407/jnpae2025.04.297

A. A. Alzubadi*, A. H. Hamade

Department of Physics, College of Science, University of Baghdad, Baghdad, Iraq

*Corresponding author: ali.abdullatif@sc.uobaghdad.edu.iq

THEORETICAL MODELING OF RADIATIVE PROTON CAPTURE IN LIGHT NUCLEI OF THE CARBON - NITROGEN - OXYGEN CYCLE USING A DIRECT CAPTURE APPROACH

The radiative proton capture reactions $^{12}C(p, \gamma)^{13}N$, $^{14}N(p, \gamma)^{15}O$, and $^{17}O(p, \gamma)^{18}F$ have been investigated within the framework of a direct capture model employing Woods - Saxon potentials. These reactions play a fundamental role in hydrogen burning through the carbon - nitrogen - oxygen (CNO) cycles in stellar interiors. Nuclear structure inputs constrained by experimental data have been used to calculate astrophysical *S*-factors and scattering phase shifts. The calculated results show good agreement with available measurements, accurately reproducing both non-resonant contributions and narrow resonance features in the $^{12}C(p, \gamma)^{13}N$ and $^{17}O(p, \gamma)^{18}F$ reactions. The rate-limiting behavior of the $^{14}N(p, \gamma)^{15}O$ reaction in the CNO-I cycle has also been described with satisfactory precision. The findings provide improved inputs for stellar nucleosynthesis modeling and contribute to the understanding of low-energy nuclear capture processes relevant to astrophysics.

Keywords: radiative proton capture, CNO nuclear cycle, astrophysical *S*-factor, direct capture model, stellar nucleosynthesis.

1. Introduction

Nuclear reactions are fundamental processes that govern both the structure of atomic nuclei and the evolution of stars [1, 2]. Among these, radiative capture reactions hold special significance for both nuclear physics and astrophysics [3]. Radiative capture involves the absorption of a projectile, such as a proton or neutron, by a target nucleus, followed by the emission of gamma radiation. These reactions play a central role in stellar energy generation and the nucleosynthesis of chemical elements in diverse astrophysical environments [4, 5].

Radiative capture reactions are broadly classified into neutron capture and proton capture. Neutron capture dominates the slow (s-) and rapid (r-) synthesis of heavier elements [6]. In contrast, proton capture reactions are central to hydrogen-burning cycles, particularly the carbon - nitrogen - oxygen (CNO) chain, which governs energy generation in stars more massive than the Sun [7, 8]. Within this cycle, reactions such as $^{13}C(p, \gamma)^{14}N$, $^{14}N(p, \gamma)^{15}O$, and $^{12}C(p, \gamma)^{13}N$ regulate the rate of energy output and influence stellar lifetimes and elemental abundances. The importance of these reactions has grown significantly since the mid-20th century, driven by advancements in detection techniques, accelerator technology, and theoretical models including R-matrix theory and statistical codes such as TALYS [9, 10].

Despite considerable progress, major challenges remain in measuring low-energy cross-sections due to the Coulomb barrier, necessitating the use of indirect methods and extrapolation techniques [11]. These uncertainties directly affect the modeling of stellar nucleosynthesis and the understanding of astrophysical phenomena. Seminal studies [12, 13] have highlighted the importance of statistically robust extrapolation methods, such as Monte Carlo uncertainty propagation and Bayesian *S*-factor analysis, in improving the reliability of low-energy reaction rate estimates for astrophysical applications. Recent efforts have also sought to reduce these uncertainties through indirect approaches and improved global optical models [14, 15]. Evaluated nuclear data libraries such as JINA REACLIB and NACRE remain crucial in this context.

In this study, a theoretical and phenomenological analysis of three key proton capture reactions $^{12}C(p, \gamma)^{13}N$, $^{14}N(p, \gamma)^{15}O$, and $^{17}O(p, \gamma)^{18}F$ has been conducted. These reactions were chosen for their crucial role in stellar hydrogen burning and their sensitivity to the physical conditions within stellar interiors. By examining these reactions, the accuracy of reaction rates and astrophysical *S*-factors used in stellar models can be improved, and deeper insights into nuclear structure phenomena such as resonance behavior and level densities near the proton threshold can be gained. These reactions were selected not only for their key roles in the CNO cycle but also because improved theoretical models can directly impact the accuracy of stellar evolution models and the predic-

tion of CNO neutrino fluxes, a topic of current interest following the first detection of solar CNO neutrinos. Moreover, these reactions serve as essential benchmarks for validating nuclear reaction theories and for providing tighter constraints in astrophysical network calculations. The ultimate goal of this work is to support a more precise determination of *S*-factors and reaction rates at stellar energies. The insights obtained are expected to enhance the predictive accuracy of nuclear reaction networks in stellar evolution models and to shed further light on the role of these reactions in stellar energy generation and elemental synthesis [12, 13].

2. Role of selected proton capture reactions in the CNO cycle

Proton-induced radiative capture reactions, specifically $^{12}C(p, \gamma)^{13}N$, $^{14}N(p, \gamma)^{15}O$, and $^{17}O(p, \gamma)^{18}F$, are recognized as key processes within the CNO cycles, which dominate hydrogen burning in stars exceeding approximately 1.3 solar masses [2]. The main branches of the CNO cycles are illustrated schematically in Fig. 1.

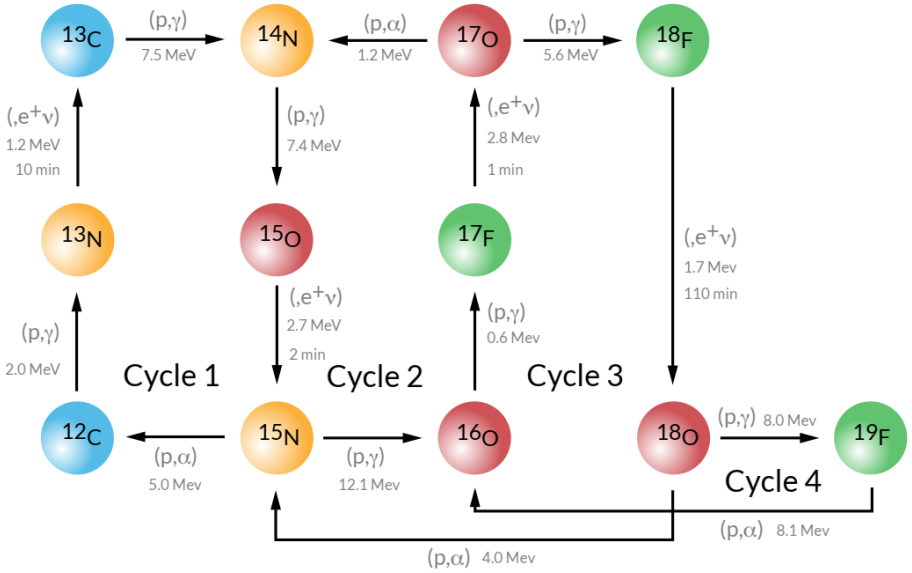

Fig. 1. The CNO cycle. (See color Figure on the journal website.)

The reaction $^{12}C(p, \gamma)^{13}N$ serves as the entry point into the CNO-I cycle, enabling the catalytic conversion of carbon into nitrogen through a sequence of proton captures and beta decays [3]. The $^{14}N(p, \gamma)^{15}O$ reaction proceeds at a significantly lower rate and represents the rate-limiting step in the cycle, thereby exerting a controlling influence on stellar energy production and neutrino fluxes [4]. In parallel, the $^{17}O(p, \gamma)^{18}F$ reaction contributes to the CNO-II branch, becoming particularly relevant at elevated stellar temperatures. This reaction affects the nucleosynthesis of fluorine isotopes and the distribution of oxygen isotopes in stellar environments [9]. Accurate determination of the cross-sections for these reactions is essential for constraining astrophysical models of stellar structure, evolution, and nucleosynthesis. The analysis of these key reactions forms the basis for the theoretical work presented in the subsequent sections.

While previous studies have extensively employed R-matrix formalism and statistical models such as TALYS, this study provides an alternative phenomenological approach that offers simplicity, computational efficiency, and sufficient accuracy for stellar modeling at low energies. The combination of phase shift analysis and direct capture (DC) formalism presented here also offers insights that complement more computationally intensive methods.

3. Theoretical consideration

Radiative proton capture reactions of the form $a + b \rightarrow c + \gamma$ constitute fundamental processes in nuclear astrophysics, particularly in stellar hydrogen burning. In these reactions, a light projectile b is absorbed by a target nucleus a, forming a compound nucleus c while emitting a gamma photon to conserve energy and angular momentum. These capture processes are responsible for both the synthesis of elements and the generation of stellar energy in environments such as the proton-proton (p-p) chain, the CNO cycles, and the s-, r-, and proton (p-) capture processes. At the low thermal energies characteristic of stellar interiors, radiative capture is predominantly governed by the DC mechanism, wherein the projectile is directly captured into a bound state without the formation of a compound nucleus. This process is theoretically described by solving the two-body Schrödinger equation for both the continuum and bound states using an effective nuclear potential. The resultant wave functions are subsequently employed

to calculate electromagnetic transition probabilities, cross-sections, and the astrophysical *S*-factor [16].

3.1. Bound state wave functions and angular momentum coupling

The total bound state wave function is defined as:

$$\Psi_{JM}\left(\vec{r}\right)=\frac{u_{lj}^{J}\left(r\right)}{r}Y_{lj}^{JM}\left(\hat{r}\right). \quad (1)$$

The term $\Psi_{JM}\left(\vec{r}\right)$ represents the total wavefunction of the system, characterized by the particular total angular momentum *J* and its associated projection M, $u_{lj}^{J}\left(r\right)$ the radial wave function, and $Y_{lj}^{JM}\left(\hat{r}\right)$ the spin-angular function, which is defined as:

$$Y_{JM}^{J}=\sum\nolimits_{m,M_a}\left\langle jm\,I_aM_a\,|\,JM\right\rangle\left|jm\right|I_aM_a\big\rangle,$$

with

$$\left|jm=\sum\nolimits_{m_l,M_b}Y_{lm_l}\left(\hat{r}\right)\chi_{M_b}, \quad (2)$$

where χ_{M_b} is the spinor wavefunction of particle *b* and $\left\langle jm\,I_aM_a\,|\,JM\right\rangle$ a Clebsch - Gordan coefficient is employed here. Radiative capture reactions are modeled within a two-body potential framework, where the interaction between the nuclei of the target and the projectile is described by the Schrödinger equation. For a bound state [17], the radial component of the time-independent Schrödinger equation is expressed as:

$$-\frac{\hbar^2}{2\mu}\left(\frac{d^2}{dr^2}-\frac{l\left(l+1\right)}{r^2}\right)u_{lj}\left(r\right)+V_{\text{eff}}\left(r\right)u_{lj}\left(r\right)=Eu_{lj}\left(r\right), \quad (3)$$

the effective potential combines central, spin-orbit, and Coulomb interactions

$$V_{\text{eff}}\left(r\right)=V_0\left(r\right)+V_{SO}\left(r\right)+V_C\left(r\right). \quad (4)$$

The central potential is defined by the Woods - Saxon (WS) form

$$V_0\left(r\right)=-V_0\left[1+\exp\left(\frac{r-R_0}{a_0}\right)\right]^{-1} \quad (5)$$

and the spin-orbit potential is expressed as:

$$V_{SO}\left(r\right)=-V_{SO}\left(\frac{\hbar}{m_\pi c}\right)^2\frac{1}{r}\frac{d}{dr}\left[1+\exp\left(\frac{r-R_{SO}}{a_{SO}}\right)\right]^{-1}\vec{l}\cdot\vec{s} \quad (6)$$

and the potential for Coulombs is defined as:

$$V_C(r)=\begin{cases}\dfrac{Z_aZ_be^2}{r}, & \text{for } r>R_C\\[2ex] \dfrac{Z_aZ_be^2}{2R_C}\left(3-\dfrac{r^2}{R_C^2}\right), & \text{for } r<R_C\end{cases}. \quad (7)$$

The parameter Zi represents the nucleus' charge number *i* (where *i* = *a*, *b*). R_C is the Coulomb radius, typically set equal to R_0. The spin-orbit interaction in Eq. 6 is formulated using the pion Compton wavelength, given as $\frac{\hbar}{m_\pi c}=1.414$ fm. The parameters V_0, V_{S0}, R_0, a_0, R_{S0}, and a_0 are carefully adjusted to reproduce the observed ground state energy E_B (or that of an excited state) [18]. The radial wavefunction is then normalized according to:

$$\int_0^\infty\left|u_{lj}\left(r\right)\right|^2dr=1. \quad (8)$$

3.2. Bound and continuum states

For bound states ($E<0$), wave functions decay at large *r*. For continuum states:

$$u_{Elj}^{J}\left(r\to\infty\right)=i\sqrt{\frac{m_{ab}}{2\pi k\hbar^2}}\left[H_l^{(-)}\left(r\right)-S_{lJ}H_l^{(+)}\left(r\right)\right]e^{i\sigma_l(E)}. \quad (9)$$

Here, $H_l^{(\pm)}\left(r\right)$ are Coulomb wavefunctions given by:

$$H_l^{(\pm)}\left(r\right)=G_l\left(r\right)\pm iF_l\left(r\right). \quad (10)$$

This expresses the Coulomb wavefunctions $H_l^{(\pm)}\left(r\right)$ as combinations of the Coulomb functions of the regular F_l and irregular G_l. σ_l is the Coulomb phase shift, and the scattering matrix is given by $S_{lJ}=e^{2i\delta_{lJ}}$, where δ_{lJ} is the nuclear phase shift. To extract the alteration in phase, the numerical solution is matched to the known asymptotic form at a matching radius *R*, using the logarithmic derivative:

$$\alpha_{lJ}=\left(\frac{du_{Elj}^{J}/dr}{u_{Elj}^{J}}\right)_{r=R}. \quad (11)$$

This leads to the scattering matrix expressed as:

$$S_{lJ}=\frac{G_l^{'}-iF_l^{'}-\alpha_{lJ}\left(G_l-iF_l\right)}{G_l^{'}+iF_l^{'}-\alpha_{lJ}\left(G_l+iF_l\right)}. \quad (12)$$

A resonance occurs when the phase shift satisfies:

$$\left.\frac{d^2\delta_{lJ}}{dE^2}\right|_{E_{lJ}^R}=0,\ \text{and}\ \left.\frac{d\delta_{lJ}}{dE}\right|_{E_{lJ}^R}>0. \quad (13)$$

The resonance width is given by:

$$\Gamma_{lJ}^{R} = 2\left(\frac{d\delta_{lJ}}{dE}\bigg|_{E_{lJ}^{R}} \right)^{-1}. \quad (14)$$

3.3. Electromagnetic transitions

Electric multipole transitions dominate radiative capture processes. The transition operator of multipolarity λμ is:

$$\mathcal{O}_{\mathcal{E}\lambda\mu} = e_{\lambda}\, r^{\lambda} Y_{\lambda\mu}(\hat{r}), \quad (15)$$

where the effective charge e_λ accounts for the center-of-mass correction:

$$e_{\lambda} = Z_b e\left(-\frac{m_a}{m_c} \right)^{\lambda} + Z_a e\left(\frac{m_b}{m_c} \right)^{\lambda}. \quad (16)$$

The reduced matrix element for a multipole transition is formally represented as:

$$\left\langle J \,\|\, \mathcal{O}_{E\lambda} \,\|\, J_0 \right\rangle = (-1)^{j+I_a+J_0+\lambda} \sqrt{(2J+1)(2J_0+1)} \begin{Bmatrix} j & J & I_a \\ J_0 & j_0 & \lambda \end{Bmatrix} \left\langle lj \,\|\, \mathcal{O}_{E\lambda} \,\|\, l_0 j_0 \rangle_J \right\rangle, \quad (17)$$

where the single-particle radial matrix element is given by

$$\left\langle lj \left\| r^{\lambda} Y_{\lambda} \right\| l_0 j_0 \right\rangle = e_{\lambda} \sqrt{4\pi} \int_0^{\infty} dr\, r^{\lambda}\, u_{lj}^{J}(r)\, u_{l_0 j_0}^{J_0}(r). \quad (18)$$

3.4. Cross-sections and astrophysical *S*-factor

The cross-section for photo-dissociation is given by:

$$\sigma_{\gamma}^{(\lambda)}(E_{\gamma}) = \frac{(2\pi)^3(\lambda+1)}{\lambda\left[(2\lambda+1)!!\right]^2} \left(\frac{m_{ab}}{\hbar^2 k} \right) \left(\frac{E_{\gamma}}{\hbar c} \right)^{2\lambda-1} \frac{dB(\pi\lambda)}{dE}, \quad (19)$$

where $E_{\gamma} = E + |E_B|$, with $|E_B|$ signifies the binding energy of the two-body system comprising particles '*a*' and '*b*'. For transitions occurring between bound states:

$$\sigma_{\gamma}^{(\pi\lambda)}(E_{\gamma}) = \frac{(2\pi)^3(\lambda+1)}{\lambda\left[(2\lambda+1)!!\right]^2} \left(\frac{E_{\gamma}}{\hbar c} \right)^{2\lambda-1} \times$$

$$\times B(\pi\lambda; l_0 j_0 J_0 \to ljJ)\, \delta(E_f - E_i - E_{\gamma}), \quad (20)$$

where E_i and E_f are the energies of the initial and final states. The radiative capture cross-section by detailed balance:

$$\sigma_{(\pi\lambda)}^{(\mathrm{rc})}(E) = \left(\frac{E_{\gamma}}{\hbar c} \right)^{2\lambda-1} \frac{2(2I_c+1)}{(2I_a+1)(2I_b+1)} \sigma_{\gamma}^{(\lambda)}(E_{\gamma}). \quad (21)$$

Summing over all allowed transitions and including spectroscopic factors (SFs) C^2S_i, the total capture cross-section σ_{nr} is given by

$$\sigma_{\mathrm{nr}}(E) = \sum_{i,\pi,\lambda} \left(C^2 S \right)_i \sigma_{(\pi\lambda),i}^{(\mathrm{rc})}(E). \quad (22)$$

As follows is the definition of the astrophysical *S*-factor for the direct acquisition of charged particles to a continuum state to a bound state:

$$S^{(c)}(E) = E\, \sigma_{\mathrm{nr}}(E)\, e^{2\pi\eta(E)},$$

$$\text{with } \eta(E) = \frac{Z_a Z_b e^2}{\hbar v}. \quad (23)$$

All numerical calculations were performed using the computational framework described in Ref. [8]. The wave functions of the bound states were obtained by numerically solving the radial Schrödinger equation employing the Numerov method in both inward and outward directions. A surface-matching technique was employed to determine the eigenenergies accurately. For continuum states, the radial equation was integrated using a Runge - Kutta algorithm, and the scattering phase shifts were extracted by matching the numerical solutions to the analytical Coulomb wave functions in the asymptotic region. Electromagnetic transition matrix elements were calculated within the single-particle approximation.

In addition to the non-resonant DC component, resonant capture and its interference with DC make essential contributions to the total radiative cross-section, particularly near narrow or isolated resonance states. To include these effects, the total capture amplitude is expressed as the coherent sum of the DC and resonant amplitudes:

$$\mathcal{A}_{\mathrm{tot}} = \mathcal{A}_{\mathrm{DC}} + \mathcal{A}_{\mathrm{res}}. \quad (24)$$

The corresponding total cross-section is therefore given by

$$\sigma(E) \propto |\mathcal{A}_{\mathrm{DC}}|^2 + |\mathcal{A}_{\mathrm{res}}|^2 + 2\mathrm{Re}\left(\mathcal{A}_{\mathrm{DC}} \cdot \mathcal{A}_{\mathrm{res}}^{*} \right), \quad (25)$$

where the first two terms represent the independent DC and resonant contributions, while the third term accounts for their mutual interference. The resonant amplitude is modeled using a single-level Breit -

Wigner form [1, 3]:

$$\mathcal{A}_{\text{res}}(E) \propto \frac{\sqrt{\Gamma_p(E)\Gamma_\gamma(E)}}{E - E_R + i\Gamma/2}, \qquad (26)$$

where E_R is the resonance energy, $\Gamma = \Gamma_p + \Gamma_\gamma$ is the total resonance width, and $\Gamma_p(E)$ and $\Gamma_\gamma(E)$ are the energy-dependent proton and gamma partial widths, respectively. The interference term $2\,\text{Re}\left(\mathcal{A}_{\text{DC}} \cdot \mathcal{A}_{\text{res}}^*\right)$ may enhance or suppress the cross-section depending on the relative phase between the two amplitudes. In the present work, this interference is treated consistently with the angular momentum coupling and electromagnetic multipole transition rules for each reaction channel. The inclusion of both the resonant and interference terms ensures that the model accurately reproduces the observed line shapes and *S*-factor energy dependence in the regions dominated by narrow resonances.

SFs were employed to scale the electromagnetic transition strengths used in calculating the radiative capture cross sections. Unless explicitly stated otherwise, SFs were assumed to be unity, reflecting the single-particle dominance typically associated with low-energy DC reactions. For the ^{12}C(p, γ)^{13}N reaction, we retain SF = 1.00 without variation, as the transition is well established in the literature to be of nearly pure single-particle character [19], and experimental data support this assumption with minimal model dependence. For the ^{14}N(p, γ)^{15}O and ^{17}O(p, γ)^{18}F reactions, we adopt SF values constrained by prior experimental and theoretical studies. Specifically, SF = 0.51 is used for ^{14}N(p, γ)^{15}O, based on shell-model and DC analyses from Schröder et al. [20], while SF = 0.85 is adopted for ^{17}O(p, γ)^{18}F in accordance with transfer reaction data reported by Newton et al. [21]. To evaluate the impact of uncertainty in SF on the calculated astrophysical *S*-factors, we conducted a sensitivity analysis assuming a ±15 % variation in the adopted SF values. The resulting changes in the zero-energy *S*-factor, *S*(0), are presented in Table 1. For the ^{14}N(p, γ)^{15}O and ^{17}O(p, γ)^{18}F reactions, the corresponding uncertainties in *S*(0) are approximately ±8 and ±7 %, respectively. These results demonstrate that while the SF contributes moderately to the overall uncertainty in *S*-factor predictions, its influence is non-negligible in the context of precision astrophysical modeling. The computed transition strengths, including the adopted SFs, were then used to evaluate radiative capture cross sections as functions of the center-of-mass energy. The corresponding astrophysical *S*-factors were derived by applying Coulomb barrier corrections using the Sommerfeld parameter [16].

Table 1. **Nuclear structure parameters for selected (p, γ) reactions**

Reaction	J_C	J_0	I_A	E_b, MeV	V_b	SF	ΔS(0) due to ±15 % SF	Relative change, %
^{12}C (p, γ)^{13}N	$1/2^-$	$p_{1/2}$	0^+	1.94	–41.65	1.00	Not applicable	N/A
^{14}N (p ,γ)^{15}O	$3/2^+$	$s_{1/2}$	1^+	0.504	–46.79	0.51	±0.06 keV·b	±8
^{17}O (p, γ)^{18}F	1^-	$d_{5/2}$	$5/2^+$	1.4	–34.58	0.85	±0.05 keV·b	±7

4. Results and discussion

The analysis of radiative proton capture reactions within the CNO cycle has been performed using the DC model outlined in Sec. 2, incorporating a WS potential framework. Standard potential parameters, as listed in Table 2, provide the input for the calculations, including the central and spin-orbit well depths, reduced radius r_0, and diffuseness a_0, which are selected based on established values validated in low-energy nuclear reaction studies. Nuclear structure inputs specific to each reaction are compiled in Table 1, including ground-state spin-parity assignments, binding energies E_b, potential depths V_b, and SF for the compound nuclei ^{13}N, ^{15}O, and ^{18}F. These parameters are essential for accurately calculating astrophysical *S*-factors and cross sections and have been chosen to maintain consistency with both theoretical expectations and available experimental data.

Table 2. **Standard WS potential parameters used in the theoretical modeling of radiative proton capture reactions, including geometric and depth parameters for central and spin-orbit potentials**

Parameter	Value	Notes
r_o	1.2 fm	Radius parameter
a_o	0.60 fm	Diffuseness
Vso	−9.8 MeV	Spin-orbit potential depth
Ro = R_C = R_{S0}	ro $(A + 1)^{1/3}$ fm	Geometric scaling with mass number

In the following subsections, each reaction will be examined individually, and the calculated observables will be systematically compared with experimental results to evaluate the accuracy of the model.

^{12}C(p, γ)^{13}N reaction. The radiative capture reaction ^{12}C(p, γ)^{13}N is one of the essential processes in the carbon - nitrogen cycle of stellar nucleosynthesis. This section presents the key physical quantities involved in modeling the reaction using the WS potential framework and systematically compares theoretical predictions with experimental data to evaluate the accuracy of the model.

Fig. 2 displays the radial dependence of the nuclear potential employed for this reaction, calculated using the WS potential. The potential demonstrates the characteristic behavior of a mean-field nuclear interaction, exhibiting a steep attractive well that reaches approximately −30 MeV near the origin and gradually approaches zero beyond a radial distance of about 6 - 7 fm. This shape captures both the strong short-range nuclear attraction and the long-range Coulomb repulsion essential for modeling bound and scattering states. The corresponding normalized radial wave function, u(r), for the ground state of the ^{13}N nucleus is shown in Fig. 3. The wave function exhibits a pronounced peak around $r \approx 3.5$ - 4.0 fm, representing the most probable separation distance between the captured proton and the ^{12}C core. The amplitude decays exponentially at larger radii, reflecting the quantum mechanical tunneling through the Coulomb barrier, a key feature governing low-energy radiative capture probabilities in stellar environments. The behavior of u(r) is consistent with the observed binding energy and the adopted SF (SF = 1.00) for this reaction, indicating a predominantly single-particle character of the capture process.

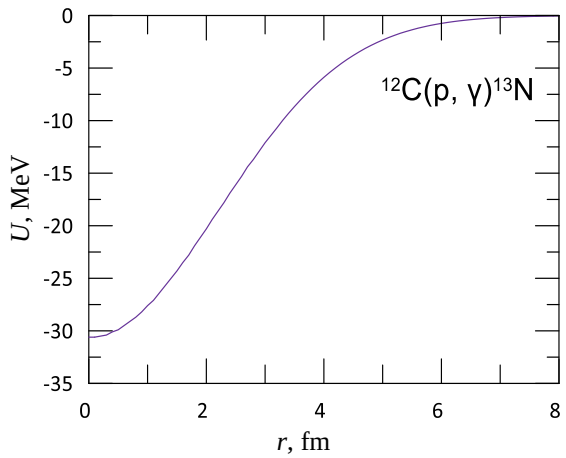

Fig. 2. WS nuclear potential U(r) for the ^{12}C(p, γ)^{13}N reaction, showing the radial dependence of the interaction. (See color Figure on the journal website.)

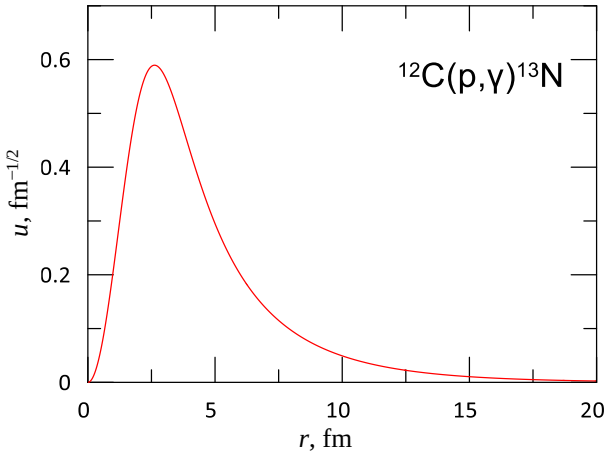

Fig. 3. Normalized radial wave function u(r) for the ^{13}N ground state in the ^{12}C(p, γ)^{13}N reaction, illustrating bound-state behavior. (See color Figure on the journal website.)

The calculated astrophysical S-factor for the ^{12}C(p, γ)^{13}N reaction as a function of the center-of-mass energy is presented in Fig. 4. The theoretical S-factor (*solid red line*) is critically compared with experimental data (open circles) from C.D. Nesaraja et al. [19]. The model reproduces the overall energy dependence and absolute scale of the S-factor across a wide energy range, including the low-energy domain (below 1 MeV) that is most relevant for stellar interiors. A pronounced resonance is observed near $E_{c.m.} = 0.422$ MeV, corresponding to the well-known $J^{\pi} = 1/2^{+}$ excited state in ^{13}N. The peak structure and magnitude of the S-factor at this energy are accurately described, confirming that the chosen WS potential parameters and SF provide a realistic depiction of the transition dynamics and nuclear structure. At energies below the resonance, the S-factor exhibits the expected exponential decline due to the Coulomb suppression of the entrance channel. The model calculations track the measured data down to approximately 0.05 MeV, demonstrating the reliability of the direct-capture formalism and the appropriateness of the potential and nuclear structure inputs. The calculated S-factor values deviate from the experimental data by less than 8 % across the energy range of 0.05 to 1 MeV, with a root-mean-square deviation of 0.07 keV·b, indicating satisfactory agreement within experimental uncertainties. Minor discrepancies at the lowest energies may be attributed to experimental errors or limitations in the treatment of subthreshold contributions, which are not explicitly modeled in the present approach.

The phase shift analysis of the elastic scattering process is shown in Fig. 5, where the energy dependence of the scattering phase shift (*solid blue line*) and its derivative (*dotted red line*) are plotted.

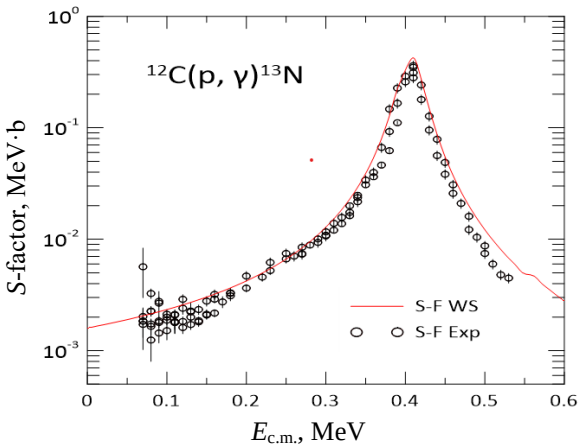

Fig. 4. Astrophysical *S*-factor for the ^{12}C(p, γ)^{13}N reaction as a function of center-of-mass energy. Theoretical results (*solid line*) are compared with experimental data (*open circles*) [19]. (See color Figure on the journal website.)

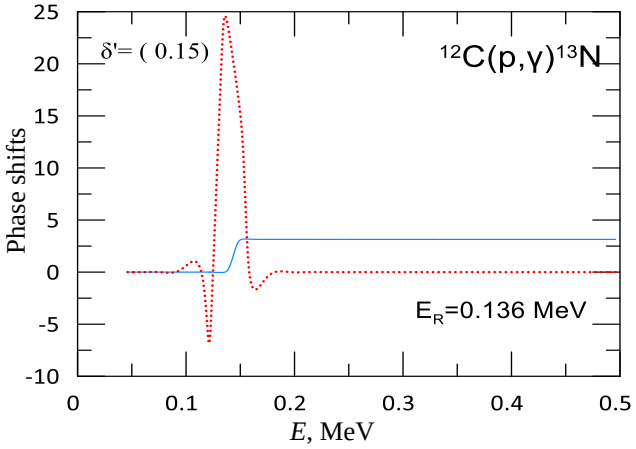

Fig. 5. Scattering phase shift and its derivative for the ^{12}C + p system, highlighting the resonance at E_R = 0.136 MeV. (See color Figure on the journal website.)

A clear resonance feature is identified near E_R = 0.136 MeV, corresponding to the same $J^\pi = 1/2^+$ state in ^{13}N responsible for the resonance in the capture cross-section. The phase shift exhibits the characteristic Breit - Wigner behavior, rapidly increasing through π/2 at the resonance energy. The sharp peak in the derivative of the phase shift provides an independent confirmation of the narrow width and long lifetime of this intermediate state. Such phase shift behavior is essential for enhancing the capture cross-section and demonstrates that the adopted WS potential reliably reproduces the resonance properties observed experimentally. The dominance of the *E*1 electromagnetic transition in this reaction arises from the favorable overlap between the incoming *p*-wave proton and the $p_{3/2}$ ground state of ^{13}N, consistent with a strong single-particle contribution. This nuclear structure feature explains the relatively high astrophysical *S*-factor observed near the resonance and highlights the sensitivity of the reaction to the details of the potential and angular momentum coupling. Overall, the theoretical model successfully captures both the resonant and non-resonant behavior of the ^{12}C(p, γ)^{13}N reaction, with implications for accurately modeling energy production in stars undergoing CNO hydrogen burning. The results reinforce the validity of using the DC approach with WS potentials to describe low-energy nuclear reactions relevant to astrophysics.

^{14}N(p, γ)^{15}O reaction. The radiative proton capture reaction ^{14}N(p, γ)^{15}O plays a crucial role in hydrogen-burning processes within stars, serving as the rate-limiting step in the CNO-I cycle. This reaction controls the overall pace of energy production in stars more massive than the Sun and directly influences CNO neutrino fluxes and stellar lifetimes. Precise modeling of this reaction is essential for accurate stellar evolution simulations and cosmological age determinations.

The calculated WS nuclear potential for the ^{14}N + *p* system is presented in Fig. 6. The potential well reaches a depth of approximately −27 MeV with a surface region near 6.5 fm. These parameters are chosen to reproduce the empirical binding energy of the ^{15}O final state and to ensure the correct asymptotic behavior of the bound-state wave function. The normalized radial wave function *u*(r) for the dominant bound state of ^{15}O ($J^\pi = 3/2^+$, Ex = 6.793 MeV) is shown in Fig. 7. The wave function exhibits a peak near r ≈ 4 fm, corresponding to the most probable separation distance between the captured proton and the ^{14}N core. The wave function decays exponentially at larger radii, reflecting the expected quantum tunneling behavior. The adoption of the SF of 0.51 for this state reflects the mixed nuclear configuration and reduced single-particle occupancy, which directly influences the magnitude of the calculated *S*-factor. This reduced SF value is consistent with previous experimental studies and shell-model calculations that indicate configuration mixing in ^{15}O.

The astrophysical *S*-factor for the ^{14}N(p, γ)^{15}O reaction is plotted in Fig. 8 as a function of center-of-mass energy. The theoretical *S*-factor (*solid line*), calculated using the WS potential and including *E*1 transitions, is compared with experimental data from multiple sources [20, 22, 23]. The model accurately reproduces both the general energy dependence and the absolute scale of the experimental *S*-factor, particularly in the sub-MeV region where DC dominates. A prominent resonance is observed at $E_{c.m.} \approx 0.259$ MeV, corresponding to the well-known $J^\pi = 1/2^+$ state in ^{15}O. This resonance enhances the *S*-factor significantly and is well captured by the theoretical model. The observed resonance arises from the constructive

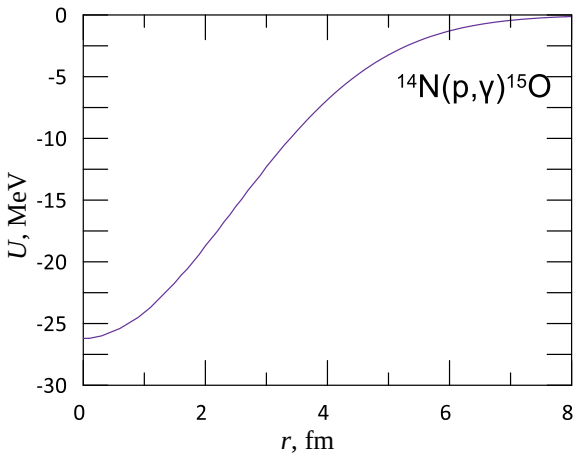

Fig. 6. WS potential $U(r)$ for the ^{14}N(p, γ)^{15}O reaction showing the radial dependence of the nuclear interaction. (See color Figure on the journal website.)

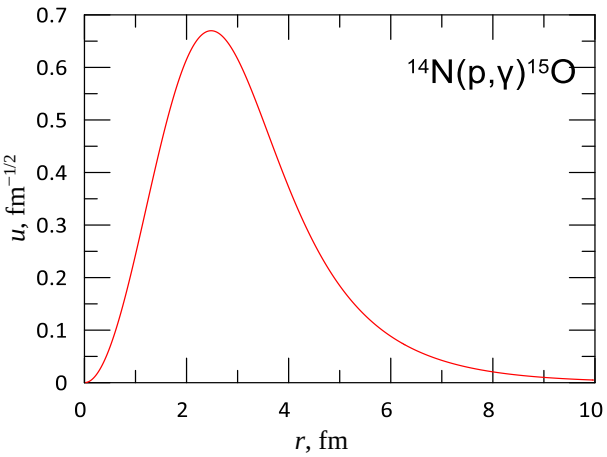

Fig. 7. Normalized radial wave function $u(r)$ for the ^{15}O bound state in the ^{14}(p, γ)^{15}O reaction. (See color Figure on the journal website.)

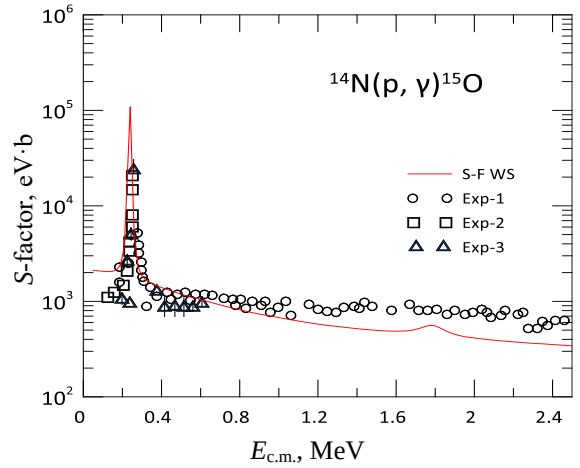

Fig. 8. Astrophysical S-factor for the ^{14}N(p, γ)^{15}O reaction as a function of center-of-mass energy. Theoretical curve (*solid line*) compared with experimental data [20, 22, 23] (*symbols*). (See color Figure on the journal website.)

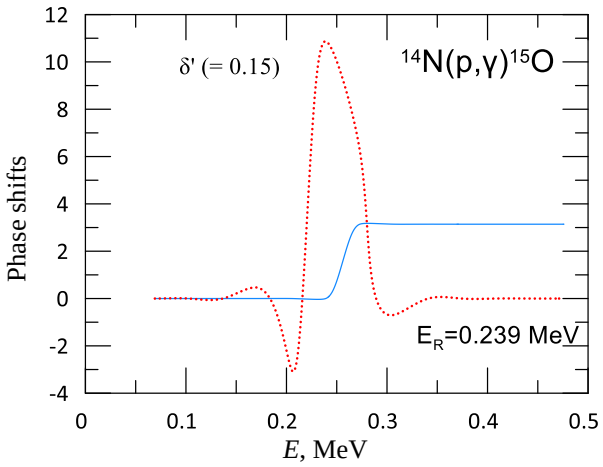

Fig. 9. Scattering phase shift and its derivative for the ^{14}N + p system, highlighting the resonance at E_R = 0.239 MeV. (See color Figure on the journal website.)

interference of the incoming s-wave proton with the bound state wave function, leading to a temporary formation of a compound state that enhances the capture cross-section. The calculated S-factor values deviate from the experimental data by less than 10 % in the energy range of 0.1 - 0.5 MeV, with a root-mean-square deviation of approximately 0.05 keV·b, demonstrating satisfactory agreement within experimental uncertainties. The non-resonant background is also well reproduced, with the reduced SF appropriately suppressing the low-energy DC cross-section. The phase shift analysis for elastic scattering in the ^{14}N + p system is shown in Fig. 9. The scattering phase shift (*solid line*) and its energy derivative (*dotted line*) reveal a clear resonance feature near E_R = 0.239 MeV. The phase shift rapidly increases through π/2 at this energy, consistent with the Breit - Wigner resonance profile, while the sharp peak in the derivative indicates a relatively narrow resonance width. The narrowness of the derivative peak suggests a long-lived intermediate nuclear state, whose properties are crucial for accurately modeling both the resonant and non-resonant capture components. Variations in the adopted WS potential parameters by ±5 % lead to corresponding changes in the calculated S-factor of approximately 8–12 % in the astrophysically relevant energy window, highlighting the sensitivity of low-energy capture cross-sections to nuclear structure inputs. Similarly, uncertainties in the SF contribute directly to the normalization of the S-factor. The accurate description of the ^{14}N(p, γ)^{15}O reaction is of particular importance for astrophysical applications. As the slowest step in the CNO cycle, this reaction rate governs the overall energy generation rate in stars with masses exceeding ~1.3 M⊙. Furthermore, it influences the production of solar CNO-cycle neutrinos, which have recently been detected by the Borexino experiment, providing a new window into stellar interiors. Improved precision in the ^{14}N(p, γ)^{15}O S-factor directly impacts age estimates of globular clusters, solar model calibrations, and the interpretation of stellar evolution timescales.

The results presented here contribute to reducing these key uncertainties and demonstrate the utility of the DC model in providing reliable inputs for astrophysical reaction networks.

^{17}O(p, γ)^{18}F reaction. The ^{17}O(p, γ)^{18}F reaction plays a central role in the nucleosynthesis pathways of the CNO-II and CNO-III cycles, contributing to the synthesis and destruction of ^{18}F in stellar environments. This reaction is of particular astrophysical interest due to the β^+ decay of ^{18}F, which can produce observable 511 keV gamma-ray signatures in classical novae and other explosive astrophysical scenarios. Accurate knowledge of the *S*-factor for this reaction is therefore essential for modeling stellar nucleosynthesis, interpreting gamma-ray observations, and constraining reaction network calculations.

The WS potential employed in the present study for the ^{17}O + *p* system is shown in Fig. 10. The potential depth of approximately −34.6 MeV and diffuseness of 0.6 fm are selected to reproduce the binding energy of the ^{18}F ground state and ensure the proper asymptotic behavior of the bound-state wave function. The radial dependence reflects the finite range of the nuclear interaction and matches established potential parameterizations used in previous low-energy capture studies.

The corresponding bound-state radial wave function, depicted in Fig. 11, exhibits a pronounced peak at approximately 3 fm and the expected exponential fall-off at large radii. This behavior underlines the importance of Coulomb barrier penetration in determining the low-energy capture probability. The wave function's spatial localization in the nuclear surface region plays a key role in defining the overlap between the initial scattering state and the final bound state.

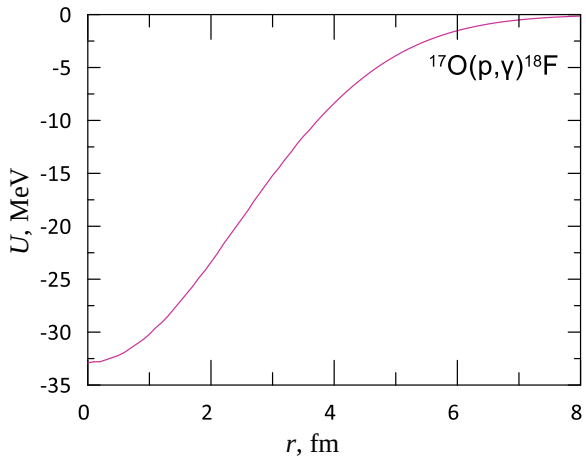

Fig. 10. Radial dependence of the WS nuclear potential *U*(r) used in the calculation of the ^{17}O(p, γ)^{18}F reaction. (See color Figure on the journal website.)

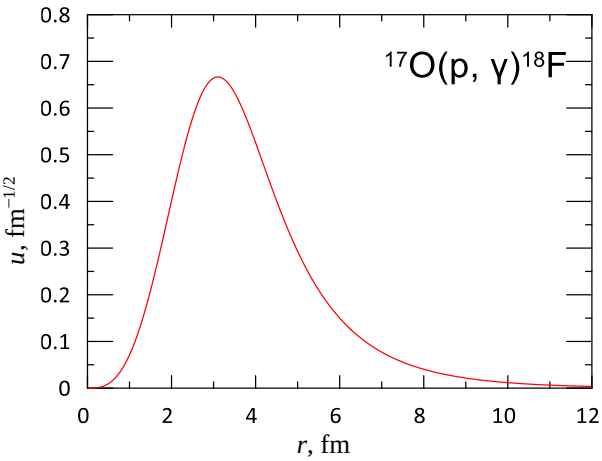

Fig. 11. Normalized radial wave function *u*(r) of the ^{18}F ground state formed in the ^{17}O(p, γ)^{18}F reaction. (See color Figure on the journal website.)

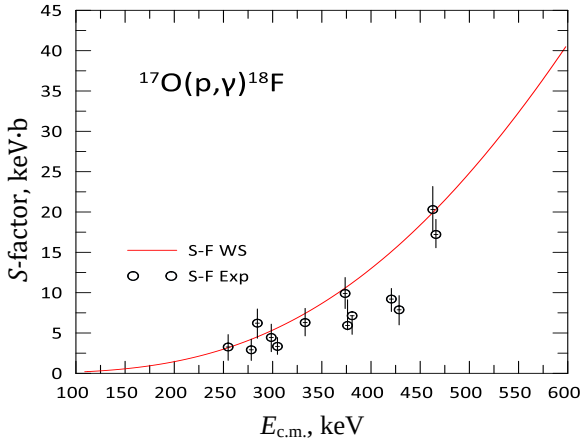

Fig. 12. Calculated astrophysical *S*-factor for the ^{17}O(p, γ)^{18}F reaction as a function of center-of-mass energy. The experimental data points are taken from Ref. [21]. A narrow resonance is observed near $E_{c.m.}$ = 0.69 MeV. (See color Figure on the journal website.)

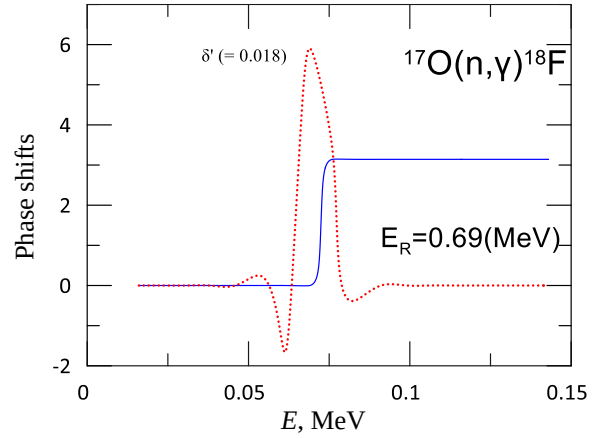

Fig. 13. Scattering phase shift and its derivative for the ^{17}O + *p* system, highlighting the resonance at E_R = 0.69 MeV. (See color Figure on the journal website.)

The calculated astrophysical *S*-factor for the $^{17}O(p, \gamma)^{18}F$ reaction is presented in Fig. 12, together with experimental data from Ref. [21]. The DC component dominates the *S*-factor at sub-MeV energies, exhibiting the expected gradual rise with increasing center-of-mass energy as the penetrability through the Coulomb barrier improves. A pronounced narrow resonance is identified at $E_n = 0.69$ MeV, corresponding to the well-known $J^\pi = 1^+$ state in ^{18}F.

The present theoretical calculations reproduce the experimental *S*-factor data with deviations of approximately 10% or less across the energy range of 100–600 keV. The root-mean-square deviation between the model predictions and the measured values is estimated to be 0.06 keV·b, confirming the adequacy of the DC model combined with the adopted nuclear structure inputs. Minor discrepancies in the energy interval 300–400 keV may arise from unaccounted low-energy resonances, interference effects between resonant and non-resonant amplitudes, or experimental systematics, as previously suggested in Ref. [21]. These discrepancies warrant further investigation using complementary experimental and theoretical microscopic approaches. The choice of spectroscopic factor SF = 0.85, constrained by independent transfer reaction studies, reflects the partial occupancy of the relevant nuclear configuration in ^{18}F and scales the calculated cross-section accordingly. This parameter ensures consistency with the observed absolute *S*-factor magnitude and underscores the sensitivity of capture probabilities to underlying nuclear structure effects.

The elastic scattering phase shift analysis is shown in Fig. 13, where the energy dependence of the scattering phase shift and its derivative reveals the narrow resonance at $E_n = 0.69$ MeV. The phase shift exhibits the characteristic Breit - Wigner rise through $\pi/2$, while the derivative displays a sharp Lorentzian peak centered at the resonance energy. The narrow width of this peak reflects a relatively long-lived intermediate state with weak coupling to the entrance channel, consistent with the small resonance width observed experimentally. The angular momentum considerations further confirm the $l = 0$ character of the entrance channel, which facilitates strong coupling to the $J^\pi = 1^+$ bound state through *E*1 transitions. Variations of the central potential depth by ±5 % lead to corresponding changes in the *S*-factor of approximately 10 % in the energy range below 600 keV. This level of theoretical sensitivity highlights the importance of accurate nuclear structure inputs, particularly the choice of potential geometry and the SF, in modeling radiative capture cross-sections at stellar energies. The accurate description of the $^{17}O(p, \gamma)^{18}F$ *S*-factor has significant implications for astrophysics. In quiescent hydrogen-burning conditions, this reaction regulates the flow between the CNO-II and CNO-III cycles and influences the isotopic abundances of oxygen and fluorine. In explosive hydrogen burning, such as in novae, the production of ^{18}F governs the early gamma-ray emission through positron annihilation. The results of this study, which provide both validated theoretical cross-sections and phase shift analyses, offer valuable inputs for updated stellar nucleosynthesis models and reaction rate libraries, such as JINA REACLIB.

5. Conclusions

In this study, we have theoretically investigated the radiative proton capture reactions $^{12}C(p, \gamma)^{13}N$, $^{14}N(p, \gamma)^{15}O$, and $^{17}O(p, \gamma)^{18}F$ using a DC model with WS potentials. These reactions are key components of the CNO cycle, which governs hydrogen burning in stars more massive than approximately 1.3–1.5 $M\odot$.

For the $^{12}C(p, \gamma)^{13}N$ reaction, the calculated astrophysical *S*-factors successfully reproduce the experimental data across the energy range 0.05–1 MeV, with a maximum deviation of less than 8 % and an RMS deviation of 0.07 keV·b. The model accurately describes the resonance at $E_{c.m.} = 0.422$ MeV, as confirmed by the phase shift analysis, which shows the characteristic behavior of a narrow resonance. The $^{14}N(p, \gamma)^{15}O$ reaction, which determines the overall rate of the CNO-I cycle, was also described with good agreement. The theoretical *S*-factor matches experimental results within 10 % below 0.5 MeV, including the reproduction of the narrow resonance near $E_{c.m.} = 0.259$ MeV. The use of a spectroscopic factor SF = 0.51 adequately reproduces the reduced non-resonant capture cross-section, and the sensitivity analysis shows that variations in the potential depth change the *S*-factor by about 8–12 %. For the $^{17}O(p, \gamma)^{18}F$ reaction, the model reproduces both the non-resonant behavior and the narrow resonance at $E_{c.m.} = 0.69$ MeV, corresponding to the $J^\pi = 1^+$ state in ^{18}F. The calculated *S*-factors deviate by less than 10 % from the experimental values, with an RMS deviation of 0.06 keV·b. The associated phase shift analysis independently confirms the presence and position of this resonance. The accurate modeling of this reaction is relevant for the synthesis of ^{18}F in novae and its observational consequences in gamma-ray astronomy.

The overall consistency between the theoretical predictions and experimental data across all three reactions demonstrates the applicability of the DC model combined with WS potentials. The results contribute to improved reaction rate inputs for stellar models, particularly for processes sensitive to the CNO cycle in both hydrostatic and explosive burning environments. Future improvements may include the use of microscopic nuclear structure models and more detailed uncertainty quantification to enhance the predictive power of the calculations.

REFERENCES

1. G.R. Satchler. *Direct Nuclear Reactions* (Oxford, Oxford University Press, 1983) 833 p.
2. K.S. Krane. *Introductory Nuclear Physics.* 3rd ed. (New York, John Wiley &Sons, 1991) 864 p.
3. C. Iliadis. *Nuclear Physics of Stars.* 2nd ed. (Weinheim-Berlin, Wiley-VCH Verlag GmbH & Co. KGaA, 2015) 654 p.
4. D.D. Clayton. *Principles of Stellar Evolution and Nucleosynthesis* (Chicago, University of Chicago Press, 1983) 634 p.
5. H.A. Bethe. Energy production in stars. Phys. Rev. 55 (1939) 434.
6. F.-K. Thielemann, M. Arnould, J.W. Truran. In: *Advances in Nuclear Astrophysics.* E. Vangioni-Flam et al. (Eds.) (Gif-sur-Yvette, Editions Frontières, 1987) p. 525.
7. C.E. Rolfs, W.S. Rodney. *Cauldrons in the Cosmos: Nuclear Astrophysics* (Chicago, University of Chicago Press 1988) 561 p.
8. J.N. Bahcall, R.K. Ulrich. Solar models, neutrino experiments, and helioseismology. Rev. Mod. Phys. 60 (1988) 297.
9. R.E. Azuma et al. AZURE: An R-matrix code for nuclear astrophysics. Phys. Rev. C 81 (2010) 045805.
10. A. Koning, S. Hilaire, S. Goriely. *TALYS-1.95: A Nuclear Reaction Program.* User Manual (The Netherlands, Petten, NRG, 2023) 562 p.
11. H. Schatz et al. rp-process nucleosynthesis at extreme temperature and density conditions. Phys. Rep. 294 (1998) 167.
12. C. Iliadis et al. Charged-particle thermonuclear reaction rates: II. Tables and graphs of reaction rates and probability density functions. Nucl. Phys. A 841 (2010) 31.
13. R. Longland et al. Charged-particle thermonuclear reaction rates: I. Monte Carlo method and statistical distributions. Nucl. Phys. A 841 (2010) 1.
14. G. Gangopadhyay, C. Lahiri. Recent advances in some nuclear properties relevant to the astrophysical r-process. Eur. Phys. J. Spec. Top. 233 (2024) 2885.
15. T. Rauscher, F.-K. Thielemann. Astrophysical reaction rates from statistical model calculations. At. Data Nucl. Data Tables 75 (2000) 1.
16. M. Dalvand, H. Khalili. Electromagnetic transition strengths on the S-factor for radiative capture proton by ^{17}O. Preprint Platform (2023) 1.
17. R.A. Radhi, A.A. Alzubadi. Study the nuclear form factors of low-lying excited states in ^{7}Li nucleus using the shell model with Skyrme effective interaction. Few-Body Syst. 60 (2019) 57.
18. A.A. Alzubadi, N.F. Latooffi, R.A. Radhi. Shell model and Hartree-Fock calculations for some exotic nuclei. Int. J. Mod. Phys. E 24 (2015) 1550099.
19. C.D. Nesaraja et al. Ratio of S factors for (p, γ) reactions on ^{12}C and ^{13}C at astrophysically relevant energies. Phys. Rev. C 64 (2001) 065804.
20. U. Schröder et al. Stellar reaction rate of ^{14}N(p, γ)^{15}O and hydrogen burning in massive stars. Nucl. Phys. A 467 (1987) 240.
21. J.R. Newton et al. Measurement of ^{17}O(p, γ)^{18}F between the narrow resonances at E_r^{lab} = 193 and 519 keV. Phys. Rev. C 81 (2010) 045801.
22. A. Formicola et al. Astrophysical S-factor of ^{14}N(p, γ)^{15}O. Phys. Lett. B 591 (2004) 61.
23. R.E. Pixley. *The Reaction Cross Section of Nitrogen-14 for Protons Between 220 and 600 keV.* Ph.D. thesis. (California Institute of Technology, Pasadena, 1957).

А. А. Алзубаді*, А. Г. Хамаде

Фізичний факультет, Науковий коледж, Багдадський університет, Багдад, Ірак

*Відповідальний автор: ali.abdullatif@sc.uobaghdad.edu.iq

ТЕОРЕТИЧНЕ МОДЕЛЮВАННЯ РАДІАЦІЙНОГО ЗАХОПЛЕННЯ ПРОТОНІВ У ЛЕГКИХ ЯДРАХ ЦИКЛУ ВУГЛЕЦЬ - АЗОТ – КИСЕНЬ З ВИКОРИСТАННЯМ МОДЕЛІ ПРЯМОГО ЗАХОПЛЕННЯ

Реакції радіаційного захоплення протонів ^{12}C(p, γ)^{13}N, ^{14}N(p, γ)^{15}O та ^{17}O(p, γ)^{18}F було досліджено в рамках моделі прямого захоплення з використанням потенціалів Вудса - Саксона. Ці реакції відіграють фундаментальну роль у горінні водню через цикли вуглець - азот - кисень (CNO) у надрах зірок. Вхідні дані про структуру ядра, з урахуванням експериментальної інформації, було використано для розрахунку астрофізичних *S*-факторів та фазових зсувів розсіювання. Розраховані результати демонструють добру відповідність з доступними експериментальними даними, точно відтворюючи як нерезонансні внески, так і вузькорезонансні особливості в реакціях ^{12}C(p, γ)^{13}N та ^{17}O(p, γ)^{18}F. Поведінку реакції ^{14}N(p, γ)^{15}O в циклі CNO-I також було описано із задовільною точністю. Результати дослідження забезпечують покращення даних для моделювання зоряного нуклеосинтезу та сприяють розумінню низькоенергетичних процесів захоплення в ядрах, що стосуються астрофізики.

Ключові слова: радіаційне захоплення протонів, ядерний цикл CNO, астрофізичний *S*-фактор, модель прямого захоплення, зоряний нуклеосинтез.

Надійшла / Received 30.07.2025